JOURNAL OF SOLID STATE CHEMISTRY 112, 113–119 (1994)

Layer-by-Layer Growth of Thin Films of the Infinite-Layer Compounds $SrCuO_2$ and $CaCuO_2$

A. Gupta, B. W. Hussey, T. M. Shaw, A. M. Guloy, M. Y. Chern, R. F. Saraf, and B. A. Scott

IBM Thomas J. Watson Research Center, Yorktown Heights, New York 10598-0218

Received November 18, 1993; accepted December 3, 1993

Epitaxial thin films of the infinite-layer compounds $SrCuO_2$ and $CaCuO_2$ have been grown in a layer-by-layer mode on (100) $SrTiO_3$ substrates by pulsed laser deposition with *in situ* monitoring using reflection high-energy electron diffraction (RHEED). While the pseudomorphic growth of $SrCuO_2$ thin films on lattice-matched $SrTiO_3$ substrates has been reported previously, we have also successfully synthesized for the first time high quality thin films of the other end-member, $CaCuO_2$, which is an important structural component of a number of cuprate superconductors. The stabilization of the infinite-layer $CaCuO_2$ has been achieved by using an epitaxial layer of the infinite-layer $SrCuO_2$ film as a chemical template for the nucleation and growth of this highly metastable phase. The oxygen concentration used during deposition and subsequent cooldown of the films has been observed to result in subtle structural modifications in the infinite-layer compounds, with substantial influence on their transport properties.

1. INTRODUCTION

A common crystallographic feature of the superconducting cuprates is the presence of two-dimensional CuO_2 sheets in their unit cells, which are considered essential for the occurrence of superconductivity in these materials. In particular, the Bi-, the Tl-, and the recently discovered Hg-based superconductors (1) all contain as part of their unit cell a variable number of CuO_2 layers and Ca ions alternately stacked along the c-axis. In general, the superconducting transition temperature (T_c) in these cuprates has been observed to increase as the number, n, of CuO_2 layers per unit cell increases from 1 to 3, before decreasing again for larger numbers. The end member ($n = \infty$) of the series, also representing the simplest structure containing corner-shared CuO_2 layers, is the parent compound $CaCuO_2$—the so-called infinite-layer structure. Since the early days of high T_c superconductivity there have been innumerable efforts at synthesizing this parent compound. Unfortunately, the tetragonal infinite-layer $CaCuO_2$ phase is thermodynamically unstable under most solid-state reaction conditions, and an orthorhombic phase of the compound composed of chains of edge-shared CuO_4 units is normally stabilized (2). In this compound the Ca ions lie between the CuO_4 chains in a site which is only partially (~85%) occupied, resulting in an incommensurate superstructure.

Siegrist *et al.* were the first to synthesize the tetragonal infinite-layer phase at ambient pressures; they had to partially substitute the larger Sr ion for Ca ($Ca_{0.86}Sr_{0.14}CuO_2$) in order to stabilize the structure (3). Since then, infinite-layer compounds have been stabilized over a much wider composition range, employing various mixed alkaline earth (Ca, Sr, Ba) substitutions, both in the bulk by high pressure synthesis, and in thin films by epitaxial growth. Using high pressure synthesis, infinite-layer compounds ranging from $Sr_{0.67}Ba_{0.33}CuO_2$ through $SrCuO_2$ to $Ca_{0.67}Sr_{0.33}CuO_2$ have been synthesized (4–6). Epitaxial thin films of the compounds $Ca_{1-x}Sr_xCuO_2$ ($0.15 \leq x \leq 1$) have been pseudomorphically stabilized at subatmospheric pressures and at comparatively low temperatures using pulsed laser deposition (PLD) and reactive sputtering (7, 8).

By utilizing appropriate doping and annealing procedures, superconductivity has also been observed in some high pressure synthesized bulk compounds. Interestingly, the infinite-layer compounds exhibit superconductivity both with n-type doping, with T_c's of ~40 K (5), and with p-type doping, with T_c's up to 110 K (6). Despite these recent successes, the structural instability of the pure infinite-layer $CaCuO_2$ phase has precluded investigation of the intrinsic and doped properties of this important end member of the high T_c superconductors.

Herein, we report on the two dimensional (2D) layer-by-layer synthesis, with thickness control on a unit-cell scale, of epitaxial films of $CaCuO_2$. This has been accomplished by first growing an epitaxial film of infinite-layer $SrCuO_2$, which is used as a chemical template for the nucleation and growth of the $CaCuO_2$ films. To the best of our knowledge, other than a brief account by Yazawa *et al.* on the sputter deposition of substantially Cu-deficient (Cu/Ca = 0.8) thin films of $CaCuO_2$ (9), this is the first report on the growth of this parent compound either in

0022-4596/94 $6.00

the bulk or in the thin film form. The ability to grow high-quality films of $CaCuO_2$ should prove valuable in investigating the electrical and magnetic properties of this model system as a function of doping. We have observed that the oxygen ambient used during deposition and cool-down produces subtle structural changes in the infinite-layer films, which have a profound influence on their transport properties, particularly in the case of $SrCuO_2$. We report results on the electrical properties of stoichiometric and cation-deficient $SrCuO_2$ and $CaCuO_2$ films prepared under different oxidizing conditions.

2. EXPERIMENTAL

The films are grown using a multitarget laser deposition system with *in situ* reflection high-energy electron diffraction (RHEED) monitoring, the details of which have been described elsewhere (10, 11). Briefly, a focused KrF excimer laser is used for ablation, with pulse energy ~40 mJ and a fluence of 2–3 J/cm^2 at the target. The (100) $SrTiO_3$ substrates are placed on a heated holder, which can be rotated and translated for proper positioning of the azimuth and incidence angles for RHEED measurements. A pulsed source of O_2 is directed at the substrate during deposition, using an electromagnetically operated pulsed valve, with the opening of the pulsed valve and the triggering of the laser synchronized with appropriate delay to ensure that the gas jet and the ablated fragments arrive at the substrate at the same time. In addition to pulsed O_2, a continuous flux of atomic O, produced downstream by microwave dissociation of O_2, is also caused to flow near the substrate through a quartz tube (atomic O flux $\simeq 10^{16}$ atoms/cm^2-sec). With the pulsed valve operating at 2–4 Hz, the background pressure in the chamber is maintained at ~1 mTorr during deposition. The Sr and Ca cuprate targets used for ablation are prepared by compaction and sintering of the powders obtained by decomposing and reacting mixtures of the appropriate precursor nitrates at 900°C in air. This preparative route does not produce the infinite-layer phase, and the Sr cuprate target has been determined by X-ray analysis to consist predominantly of the thermodynamically stable $SrCuO_2$ orthorhombic phase, whereas the Ca cuprate target is observed to be a homogenous mixture of Ca_2CuO_3 and CuO. In this paper we refer to the infinite-layer phase films prepared using these two targets as $SrCuO_2$ and $CaCuO_2$, respectively. The cation stoichiometry of some of the films has been checked using Rutherford backscattering spectroscopy (RBS), and was found to be within 5% of the nominal target composition. However, the oxygen composition of the films has not been determined, and it is likely that they are not always stoichiometric in oxygen, particularly in cases when the films are cooled down in atomic oxygen or at very low O_2 pressures.

Before deposition of the cuprate films, the (100) $SrTiO_3$ substrates are heated to 750°C and the surface is cleaned, using a 150-eV Ar-ion beam. This is followed by homoepitaxial deposition of a 100–200 Å thick buffer layer of $SrTiO_3$. The growth of the buffer layer ensures a very smooth substrate surface, which is essential for subsequent layer-by-layer growth and observation of RHEED oscillations during deposition of the cuprate films (11). With a few specific exceptions, all the films of the infinite-layer phase are grown at a substrate temperature of 500°C, with a deposition rate of ~0.1 Å/pulse and total film thickness in the range 500–1000 Å. Following deposition, the films are slowly cooled down to room temperature either in the presence of atomic O, or under various O_2 background pressures ($\leq 10^{-6}$–760 Torr), to control the film oxygen stoichiometry.

3. RESULTS AND DISCUSSION

During the growth of the first few monolayers of $SrCuO_2$ the RHEED pattern, although remaining streaky, becomes quite weak, possibly because of initial changes in the surface atomic arrangements. This makes it difficult to observe RHEED intensity oscillations during the initial growth period. However, with increasing film thickness, the intensity improves dramatically, and intensity oscillations are clearly observed during deposition. While these oscillations become damped quite rapidly, they can be reinitiated if the growth is interrupted for a brief period to allow the intensity to recover to its original value. In the context of the step-edge scattering model, the oscillations are damped and eventually disappear when the surface achieves a limiting equilibrium concentration of steps (12). This occurs when it is favorable for the arriving adatoms to migrate over a short distance and to attach to step edges, rather than to nucleate as separate 2D islands on the terraces. The recovery normally observed on interruption of growth has been attributed to the reduction of steps and the formation of effectively larger terraces because of surface migration (12). This results in reinitiation of the oscillations with subsequent growth.

To determine the growth unit corresponding to the period of the RHEED intensity oscillations, we have deposited an ultrasmooth film of $SrCuO_2$ at a slow growth rate by employing an automated sequence of monolayer deposition and then growth interruption by a fixed time interval (30 sec) to allow surface recovery. The film thickness has been independently determined after deposition using low-angle X-ray reflection. From the positions of the specularly reflected finite size X-ray peaks (10 orders of which have been observed for 2Θ below 1.5°) the thickness has been determined to be 945 ± 10 Å. This is very close to the thickness (955 Å) estimated from the number of

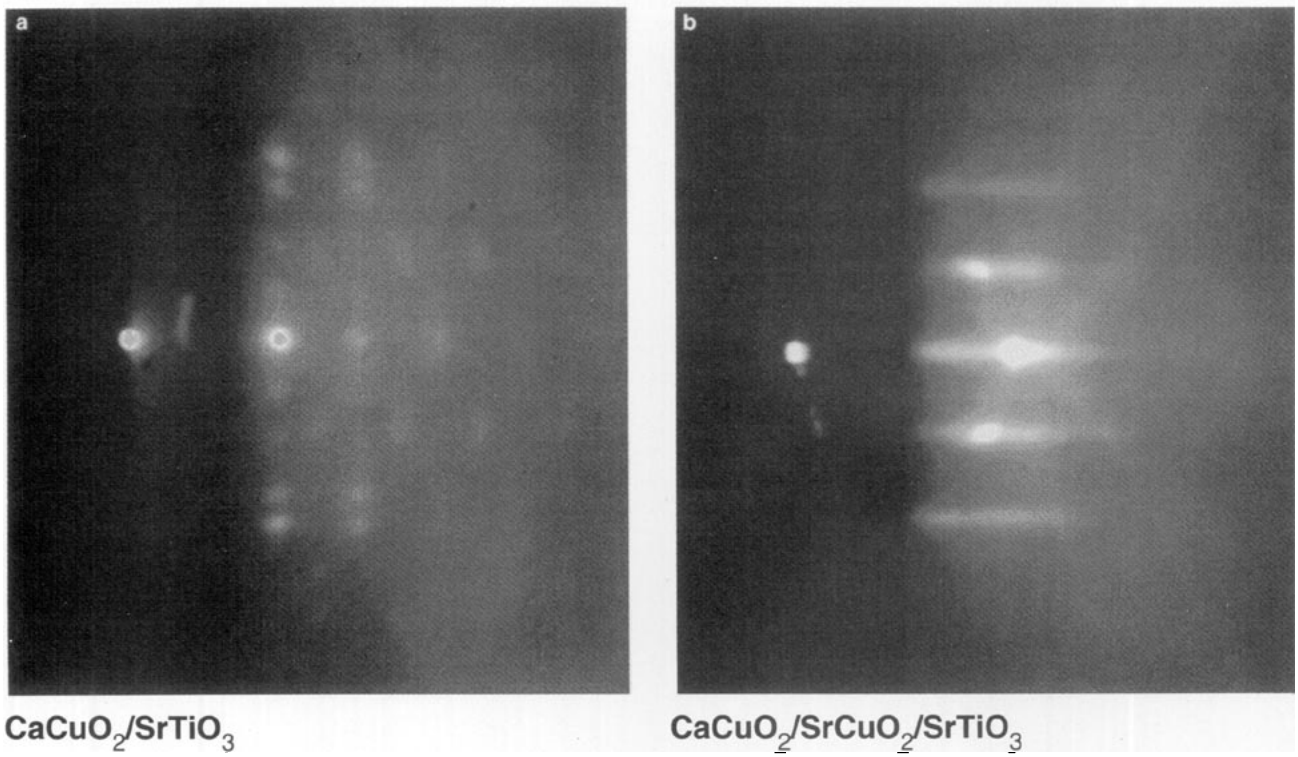

FIG. 1. RHEED patterns observed during growth of $CaCuO_2$ films at 500°C (a) when deposited directly on (100) $SrTiO_3$ substrate, and (b) after growth of a few monolayers of epitaxial infinite-layer $SrCuO_2$ film. Beam azimuth [100], beam energy 10 keV.

oscillation cycles used for the deposition, assuming that the growth unit is a single unit cell (3.47 Å). The monolayer growth thickness corresponds to the minimum unit of the infinite-layer structure which is needed to satisfy the chemical composition and electrical neutrality criteria (13).

In contrast to $SrCuO_2$, the direct deposition of Ca cuprate films on (100) $SrTiO_3$ substrates results in a drastic reduction in the RHEED beam intensity and the development of a diffuse and spotty ring pattern very quickly after the initiation of growth, which remains essentially unchanged throughout the deposition process. This suggests that the film grows with random in-plane orientation and may be poorly crystallized. A typical RHEED pattern observed for a $CaCuO_2$ film deposited directly on the substrate is shown in Fig. 1a. In contrast, we have observed that if the growth of Ca cuprate is initiated after first depositing even a few monolayers of $SrCuO_2$, then the RHEED pattern remains sharp and streaky, and in fact, some increase in the intensity of the streaks and the associated Kikuchi lines is observed during the initial stages of growth. The RHEED pattern of a film grown in this manner is shown in Fig. 1b. The streaky pattern is maintained with increasing film thickness and strong intensity oscillations of the spots of the zero-order Laue zone are clearly observed during deposition, as shown in Fig. 2. With interruption of the growth there is substantial recovery of the intensity. The deposition–recovery cycle can be repeated almost indefinitely, indicating that the quality of the deposit does not degrade with thickness. Assuming that the substrate surface, after deposition of the buffer layer, is terminated in a TiO_2 layer (10), it is expected that, during deposition of $SrCuO_2$, a layer

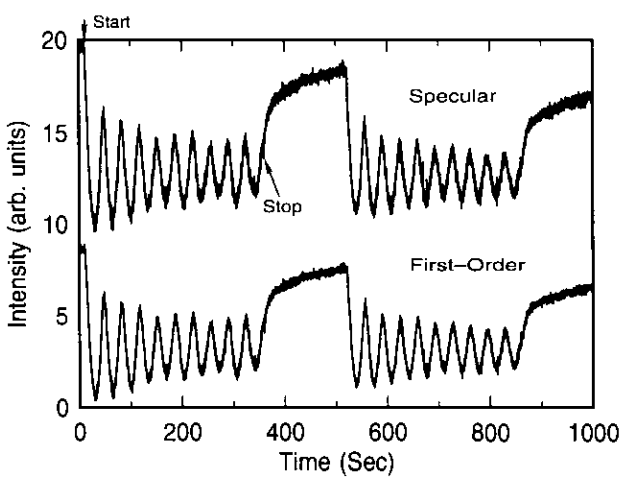

FIG. 2. Intensity oscillations of the specular and first-order diffracted spots in the RHEED pattern during growth of an infinite-layer $CaCuO_2$ film on (100) $SrTiO_3$ substrate with intermediate $SrCuO_2$ layer.

containing Sr atoms will grow first, followed by the CuO_2 layer. We speculate that the terminating CuO_2 layer of $SrCuO_2$ acts as a seed in promoting the nucleation and replication of the infinite-layer structure during the subsequent deposition of the $CaCuO_2$ film.

Figures 3a and 3b show the cross-sectional transmission electron microscopy images of Ca cuprate films grown on a $SrTiO_3$ substrate with and without an intermediate $SrCuO_2$ layer, respectively. The corresponding electron diffraction patterns, taken from the substrate and the film, with the beam aligned along the ⟨100⟩ direction of the substrate, are shown as insets. It is apparent from the image and the diffraction pattern in Fig. 3a that the direct deposition of Ca cuprate on the substrate results in the formation of a fine-grained polycrystalline film which is textured. The weak arc reflections can be indexed on the basis of $CaCuO_2$ grains with their c-axis either in the plane or normal to the substrate. The square net of stronger reflections arise from the $SrTiO_3$ substrate. On the other hand, the film deposited using a $SrCuO_2$ intermediate layer is epitaxially aligned with the substrate. The stronger spots in the diffraction pattern in Fig. 3b can be indexed on the basis of an epitaxial infinite-layer film with its a- and b-axes aligned with the cube axes of the substrate and the c-axis normal to the substrate. The lattice spacings normal and parallel to the substrate surface were measured to be ~3.16 and 3.86 Å, respectively, and are in good agreement with the c- and a-axis lengths calculated from the X-ray diffraction pattern of the film, as described later. The $SrCuO_2$ layer, used for seeding the growth, is

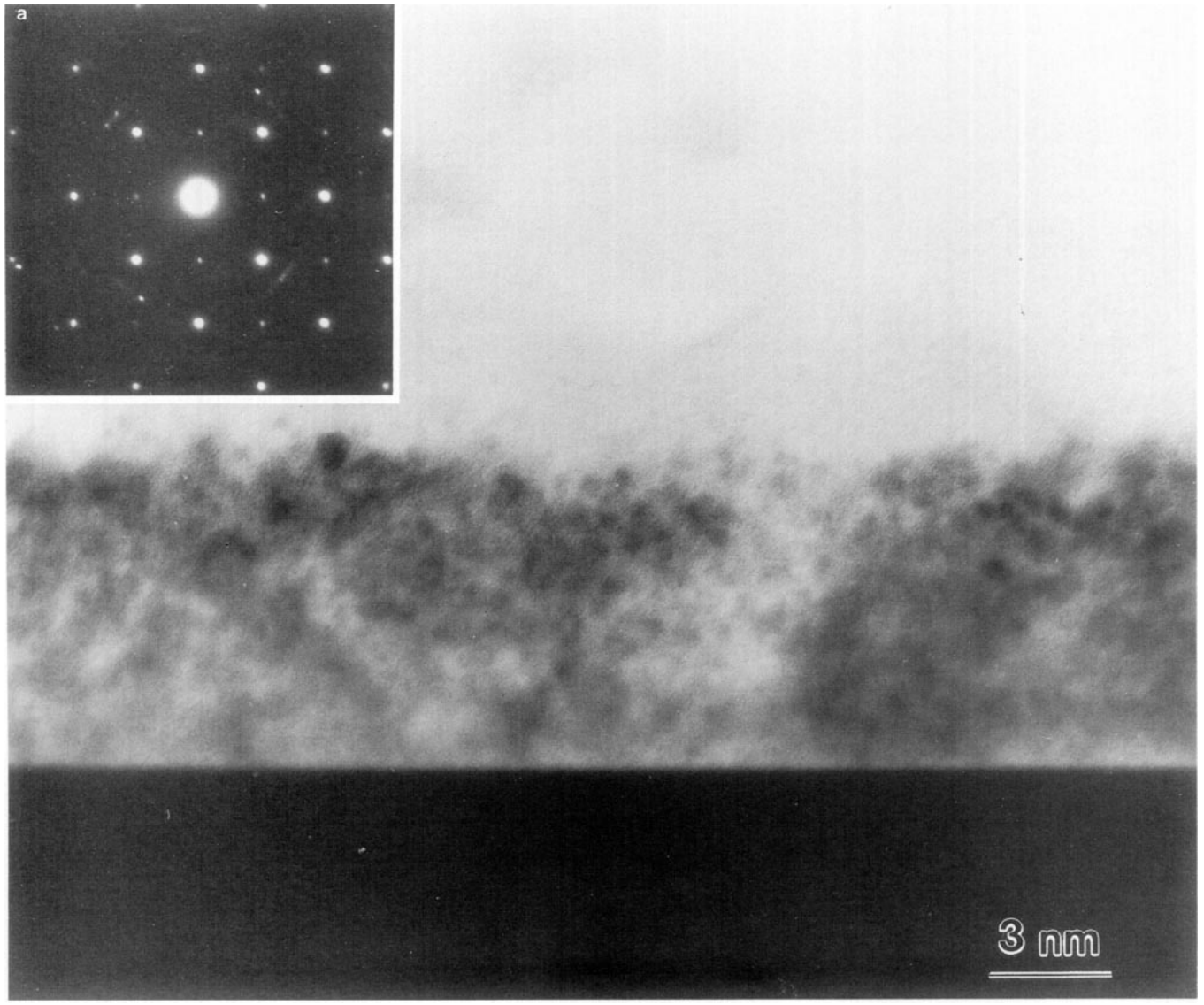

FIG. 3. Cross-section TEM micrographs and corresponding electron diffraction patterns for $CaCuO_2$ films grown (a) directly on (100) $SrTiO_3$ substrate and (b) with intermediate $SrCuO_2$ layer. Both the films were cooled under 760 Torr O_2 after deposition.

visible in Fig. 3b as a layer of darker contrast just above the $SrTiO_3$ buffer layer. Several vertical striations are evident in the image of the $CaCuO_2$ portion of the film. High-resolution imaging shows that these are stacking faults on the (100) planes of the structure.

We have also investigated the structural properties of the films as a function of oxygen annealing conditions using X-ray diffraction. The X-ray patterns in the normal Bragg-reflection geometry for the $CaCuO_2$ films cooled in atomic O and in 760 Torr O_2 are shown in Figs. 4a and 4b, respectively. Additionally, the diffraction patterns for $SrCuO_2$ films deposited and cooled under essentially identical conditions are shown in Figs. 4c and 4d. Both the $CaCuO_2$ and $SrCuO_2$ films can be indexed as tetragonal infinite-layer phases with the c-axis oriented normal to the plane of the substrate. The lattice parameter for the $CaCuO_2$ film deposited on the $SrCuO_2$ template layer and subsequently cooled in atomic O is determined to be 3.21 Å. A small decrease in the c-axis parameter of the films is observed when the films are annealed in O_2, with films cooled in 760 Torr O_2 (Fig. 4b) exhibiting a lattice parameter of 3.18 Å. We have also deposited cation-deficient $Ca_{0.9}CuO_2$ films under similar process conditions and observed no significant differences in their diffraction patterns or their c-axis lengths, as compared to the stoichiometric films. On the other hand, while the X-ray patterns for the Ca cuprate films directly deposited on $SrTiO_3$ (not shown in the figure) are qualitatively simi-

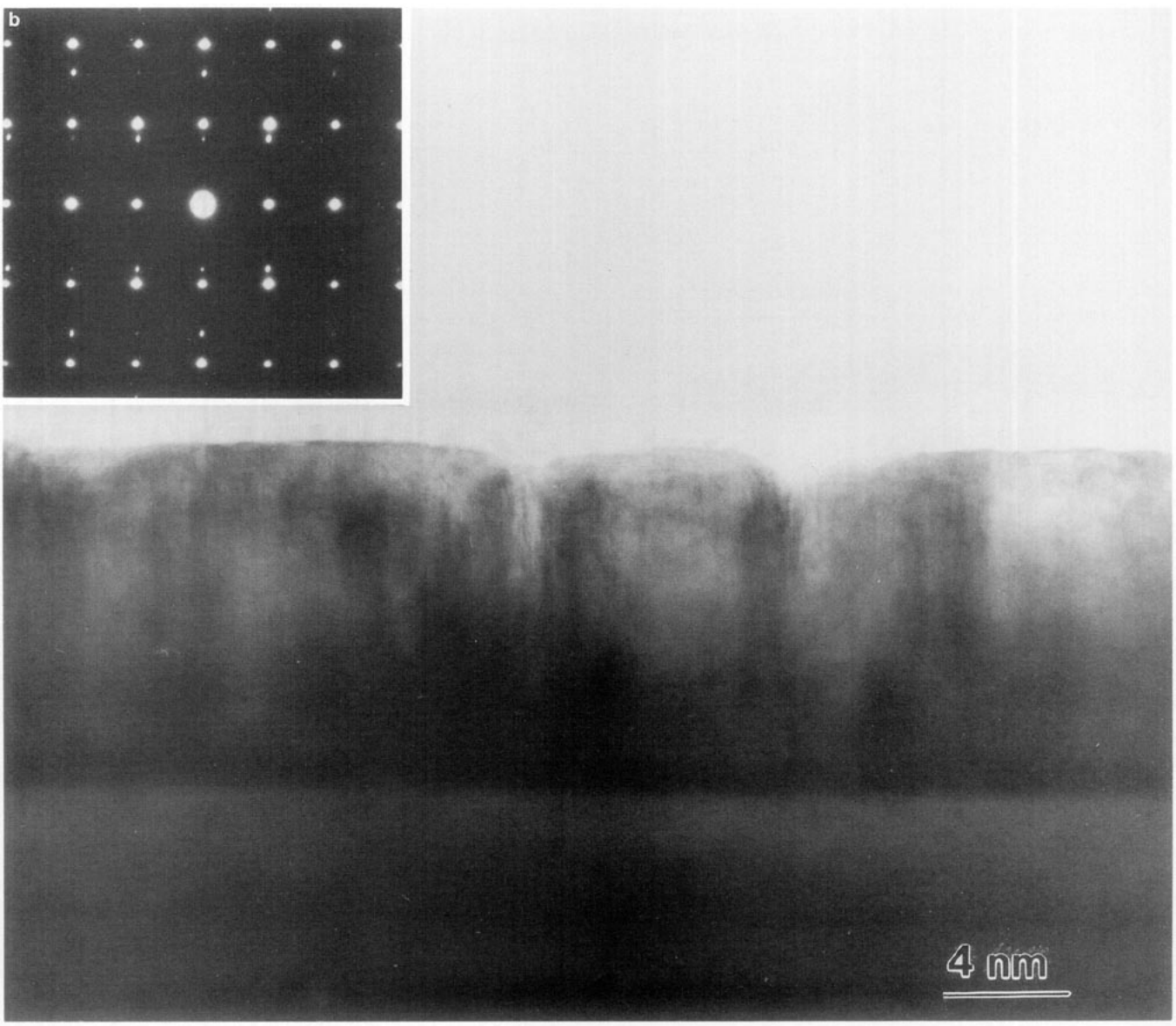

FIG. 3—*Continued*

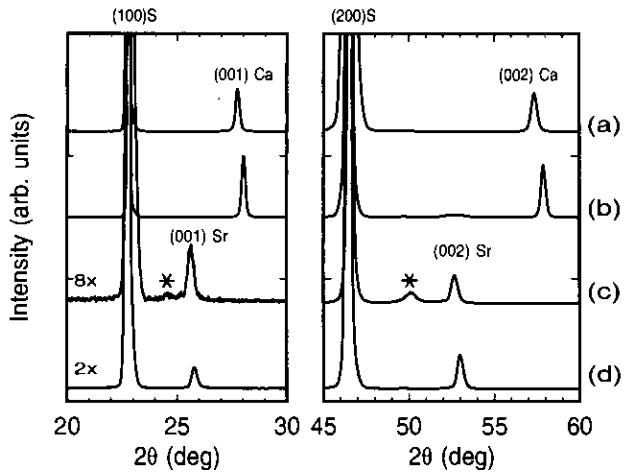

FIG. 4. X-ray diffraction patterns of $CaCuO_2$ and $SrCuO_2$ films: (a) $CaCuO_2$ film cooled under atomic O, (b) $CaCuO_2$ film cooled under 760 Torr O_2, (c) $SrCuO_2$ film cooled under atomic O, and (d) $SrCuO_2$ film cooled under 760 Torr O_2. The substrate reflections are denoted by S.

lar to those discussed above, the peaks are broader and can be indexed to a somewhat smaller lattice parameter of 3.15 Å. Unlike the infinite-layer phase films, no variation in the lattice parameter has been observed as a function of oxygen concentration during cooldown for these films.

For the $SrCuO_2$ films the c-axis lattice parameter for films cooled in atomic oxygen is determined to be 3.47 Å. Additional first- and second-order diffraction peaks, which can be indexed to a much longer lattice parameter (3.62–3.64 Å), are also observed for these films (indicated by * in Fig. 4c). Interestingly, when the films are cooled down in a high pressure O_2 ambient (or when the atomic O cooled films are post-annealed in O_2) then these low-angle peaks completely disappear, while the c-axis length corresponding to the primary infinite-layer diffraction peaks is reduced to 3.45 Å.

Resistivity versus temperature results for the $SrCuO_2$ and $CaCuO_2$ films deposited in atomic O at 500°C, and then cooled down in different oxygen ambients, are displayed in Fig. 5. We have observed that the resistivity of $SrCuO_2$ films is very sensitive to the oxygen concentration. Films cooled in low oxygen partial pressures show relatively low room-temperature resistance values (as seen for the vacuum-annealed film in Fig. 5), with a progressive increase in the resistance at higher oxygen concentrations. Moreover, films cooled in atomic oxygen, which provides a high oxygen activity, exhibit low resistivity. As seen in Fig. 5, the $SrCuO_2$ film cooled in atomic O has a room-temperature resistivity of $\sim 5 \times 10^{-3}$ Ω-cm, and exhibits semimetallic behavior as a function of temperature. On the other hand, the film cooled in 760 Torr O_2 is more resistive by at least two orders of magnitude and displays insulating characteristics. The resistance behavior of the Sr-deficient $Sr_{0.9}CuO_2$ films has been observed to be quite similar to the stoichiometric films, with about an order of magnitude lower room-temperature resistivity for the films annealed in 760-Torr O_2. Unlike the $SrCuO_2$ films, the resistance characteristics of the $CaCuO_2$ films is much less sensitive to the oxygen ambient used during the cooldown cycle. Independent of the oxygen concentration, the $CaCuO_2$ films are highly resistive, with only slight variations in their resistivity values (Fig. 5). Similar behavior has also been observed for Ca-deficient $Ca_{0.9}CuO_2$ films. The resistivities of the Ca films plotted in Fig. 5 were obtained after subtracting the resistance contribution of the Sr template layer in these films. No evidence of superconductivity has been observed down to 5 K in any of the infinite-layer phase films we have studied.

It is apparent from the above results that, in spite of their structural simplicity, the properties of the infinite-layer phase films are quite sensitive to the process conditions, particularly in the case of $SrCuO_2$, with the larger alkaline earth cation. The wide variations in the resistivity of $SrCuO_2$ as a function of oxygen concentration are possibly caused by lattice defects or imperfections. It is likely that excess oxygen can be introduced in the Sr layer when the films are cooled in the presence of atomic O. On the other hand, low oxygen concentration during cooldown can result in oxygen vacancies in the CuO_2 sheets (6).

Kasowski *et al.* (14) have computed the electronic band structures of both the orthorhombic and tetragonal (infinite-layer) phases of $CaCuO_2$ using the spin polarized, full potential pseudofunction (PSF) method. While the band structure for the orthorhombic lattice (2) renders the material insulating and the bands are very narrow near the Fermi energy, resulting in a large magnetic moment (0.58 μ_B) at the Cu atoms, the perfect tetragonal phase is

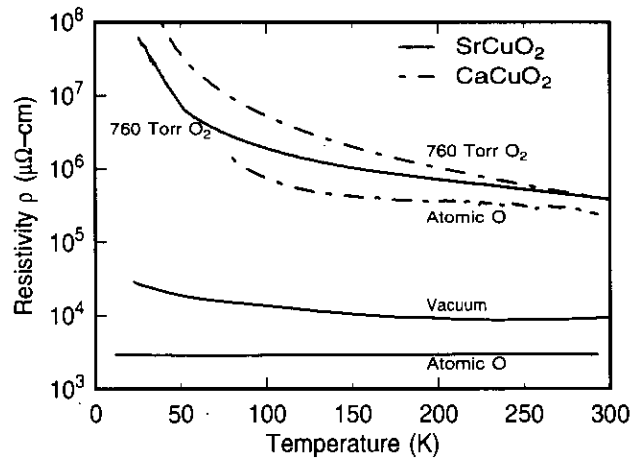

FIG. 5. Resistivity vs temperature of $SrCuO_2$ and $CaCuO_2$ films deposited at 500°C and cooled in different oxygen ambients. The corresponding X-ray diffraction patterns are shown in Fig. 4.

incorrectly predicted to be metallic. An insulating antiferromagnetic ground state is obtained for the latter only if the structure is distorted, with some of the oxygen atoms in CuO_2 sheets being displaced to occupy interplanar defect sites in the Ca plane. Interestingly, when the interplane model is repeated with partial substitution of Sr for the Ca atoms, it is observed that, as the distance between the planes (c-axis) increases with increasing Sr substitution, the bands became semimetallic, with some overlap (14). It will be useful to carry out similar calculations for the infinite-layer defect phases containing random oxygen vacancies in the sheets, and also as a function of cation doping. The effect of trivalent ion (Nd^{+3}, Sm^{+3}, and Y^{+3}) substitution on the properties of $CaCuO_2$ films is currently being investigated.

REFERENCES

1. S. N. Putilin, E. V. Antipov, O. Chmaissem, and M. Marezio, *Nature* **362,** 226 (1993); A. Schilling, M. Cantoni, J. D. Guo, and H. R. Ott, *Nature* **363,** 56 (1993).
2. T. Siegrist, R. S. Roth, C. J. Rawn, and J. J. Ritter, *Chem. Mater.* **2,** 192 (1990); T. G. N. Babu and C. Greaves, *Mater. Res. Bull.* **26,** 499 (1991).
3. T. Siegrist, S. M. Zahurak, D. W. Murphy, and R. S. Roth, *Nature* **334,** 231 (1988).
4. M. Takano, Y. Takeda, H. Okada, M. Miyamoto, and K. Kusaka, *Physica C* **159,** 375 (1989).
5. M. G. Smith, A. Manthiram, J. Zhou, J. B. Goodenough, and J. T. Market, *Nature* **351,** 549 (1991).
6. Z. Hiroi, M. Azuma, M. Takano, and Y. Takeda, *Physica C* **208,** 286 (1993); M. Azuma, Z. Hiroi, M. Takano, Y. Bando, and Y. Takeda, *Nature* **356,** 775 (1992); M. Takano, M. Azuma, Z. Hiroi, Y. Bando, and Y. Takeda, *Physica C* **176,** 441 (1991).
7. D. P. Norton, B. C. Chakoumakos, J. D. Budai, and D. H. Lowndes, *Appl. Phys. Lett.* **62,** 1679 (1993); C. Niu and C. M. Lieber, *J. Am. Chem. Soc.* **114,** 3570 (1992); X. Li, M. Kanai, T. Kawai, and S. Kawai, *Jpn. J. Appl. Phys.* **31,** L217 (1992).
8. Y. Terashima, R. Sato, S. Takeno, S. Nakamura, and T. Miura, *Jpn. J. Appl. Phys.* **32,** L48 (1993); N. Sugii, M. Ichikawa, K. Kubo, T. Sakurai, K. Yamamoto, and H. Yamauchi, *Physica C* **196,** 129 (1992).
9. I. Yazawa, N. Terada, K. Matsutani, R. Sugise, M. Jo, and H. Ihara, *Jpn. J. Appl. Phys.* **29,** L566 (1990).
10. M. Y. Chern, A. Gupta, B. W. Hussey, and T. M. Shaw, *J. Vac. Sci. Technol. A* **11,** 637 (1993).
11. M. Y. Chern, A. Gupta, and B. W. Hussey, *Appl. Phys. Lett.* **60,** 3046 (1992).
12. J. Zhang, J. H. Neave, B. A. Joyce, P. J. Dobson, and P. N. Fawcett, *Surf. Sci.* **231,** 379 (1990).
13. T. Terashima, Y. Bando, K. Iijima, K. Yamamoto, K. Hirata, K. Hayashi, K. Kamigaki, and H. Terauchi, *Phys. Rev. Lett.* **65,** 2684 (1990).
14. R. V. Kasowski, S. Hatta, and W. Y. Hsu, *Solid State Commun.* **85,** 837 (1993); S. Hatta, R. V. Kasowski, and W. Y. Hsu, *Appl. Phys. A* **55,** 508 (1992).